Hindawi Publishing Corporation
Science and Technology of Nuclear Installations
Volume 2016, Article ID 4720685, 6 pages
http://dx.doi.org/10.1155/2016/4720685

Research Article

Prediction Study on PCI Failure of Reactor Fuel Based on a Radial Basis Function Neural Network

Xinyu Wei, Jiashuang Wan, and Fuyu Zhao

School of Energy and Power Engineering, Xi'an Jiaotong University, Xi'an, Shaanxi 710049, China

Correspondence should be addressed to Xinyu Wei; xyu.wei@yahoo.com

Received 24 December 2015; Revised 11 February 2016; Accepted 10 April 2016

Academic Editor: Alejandro Clausse

Pellet-clad interaction (PCI) is one of the major issues in fuel rod design and reactor core operation in water cooled reactors. The prediction of fuel rod failure by PCI is studied in this paper by the method of radial basis function neural network (RBFNN). The neural network is built through the analysis of the existing experimental data. It is concluded that it is a suitable way to reduce the calculation complexity. A self-organized RBFNN is used in our study, which can vary its structure dynamically in order to maintain the prediction accuracy. For the purpose of the appropriate network complexity and overall computational efficiency, the hidden neurons in the RBFNN can be changed online based on the neuron activity and mutual information. The presented method is tested by the experimental data from the reference, and the results demonstrate its effectiveness.

1. Introduction

The reactor core of Light Water Reactors (LWRs) holds fuel assemblies of fuel rods, which consist of zirconium alloy tubes containing uranium dioxide pellets. The Zr-alloy cladding is the first containment barrier for fission products. Due to water pressure, the cladding creeps down until contact with the pellet occurs after a few operating cycles. In the case of a power increase, this Pellet-Cladding Interaction (PCI) induces large stresses in the cladding that might lead to fuel rod failure [1]. PCI-induced clad tube failure is caused by a combination of stresses in the Zr-alloy clad due to the pellet-clad contact pressure and chemical reaction of corrosive fission products, such as iodine released during operation, with Zr-alloy under a power ramp. If the induced stresses in the clad are sufficiently large and the concentration of the fission product is high, clad failure may occur [2, 3]. PCI has been a topic of numerous experimental and computational studies with a great amount of accumulated field experience. This has led to PCI-resistant designs and operation guidelines, which have dramatically reduced the propensity for such failures in recent years. Overviews, from industrial perspective, on PCI testing and computations relating to reactor fuels can be found in the literatures [4, 5].

It is well known that the development of the crack before clad failure is difficult to detect. The usual methods for calculating PCI mainly are finite elements models [6–8]. Nevertheless, the probability of PCI failure is hard to assess. The present study aims at this purpose. In this paper, we present a neural network method to predict PCI failure. The reduction of the calculation complexity of the present method may contribute to the online calculation and prediction of the PCI failure in operating reactors. The transients will be calculated during the entire lifetime of the pins and for each of them the PCI failure probability will be predicted. Firstly, the radial basis function neural network (RBFNN) will be trained by sufficient experimental data. Before a transient, the PCI failure probability (failure or not) will be predicted by the trained network. After the transient, the actual result and its inputs will be used to replace one of the initial experimental data; then a new RBFNN will be trained by the new data. In this way, after every transient, the REFNN will be retrained. In this study, a self-organized one RBFNN is used, which can vary its structure dynamically in order to maintain its accuracy. The hidden neurons in the RBFNN can be added or removed online based on the neuron activity and mutual information, to achieve the appropriate network complexity and maintain overall computational efficiency. In this

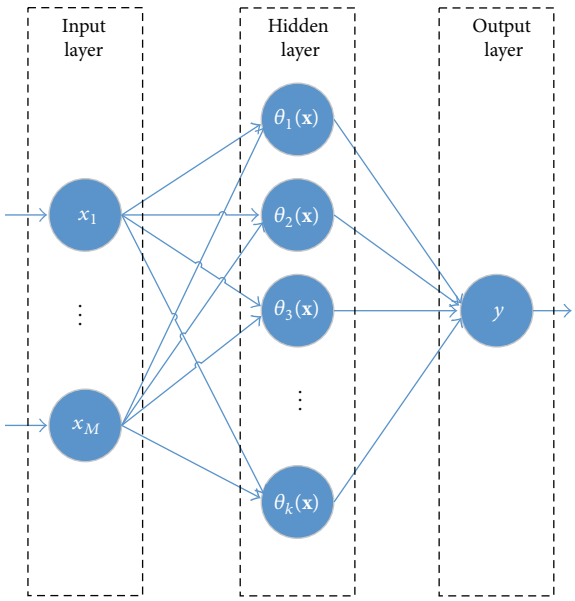

Figure 1: The structure of radial basis function neural network (RBFNN).

manner, the PCI failure probability can be predicted online by the simple and fast neural network method, which allow for straightforward implementation within a transient analysis methodology and core monitoring systems, and only the input parameters of the transient are considered in this method.

This paper is structured as follows. Section 2 illustrates the design of the self-organized RBFNN. Section 3 presents the calculation process of the PCI failure probability. The calculation results are discussed in Section 4. Finally, conclusion is given in Section 5.

2. A Self-Organized RBFNN

Taking into account that the performance of an RBFNN is heavily dependent on its architecture, many researchers have focused on self-organizing methods that can be used to design the architecture of three-layered RBFNN. In order to design the structure of the RBFNN automatically, Han et al. [9] presented a flexible structure radial basis function neural network (FS-RBFNN) by using a dynamic tuning strategy. The strategy changes the topology of the RBFNN by measuring the average firing rate of the neurons and the mutual information (MI) in the training process. The firing rate is similar to the spiking frequency of the presynaptic neuron in the biological neural system [10]. When the rate value of the hidden neuron is bigger than a given threshold value, new neurons will be inserted into the hidden layer. MI is used to measure the connectivity of hidden neurons and to obtain the connectivity between hidden neurons [11].

2.1. Radial Basis Function Neural Network. Figure 1 shows the structure of a basic RBFNN consisting of one input layer, one output layer, and one hidden layer [12]. In order to simplify the discussion, the RBF model used for analysis is multi input and single output (MISO). A single-output RBFNN with k hidden layer neurons can be described by

$$y = \sum_{k=1}^{K} \omega_k \theta_k (\mathbf{x}), \tag{1}$$

where $\mathbf{x} = (x_1, x_2, \ldots, x_M)^T$ denotes the input of the network, M is the number of input variables, y denotes the output of the network, $\omega = [\omega_1, \omega_2, \ldots, \omega_K]$ is the connecting weights between the hidden neuron and the output layer, and $\theta_k(\mathbf{x})$ is the output value of the kth hidden neuron and can be calculated by

$$\theta_k (\mathbf{x}) = \exp\left(-\frac{\|\mathbf{x} - \mu_k\|}{\sigma_k^2} \right), \tag{2}$$

where μ_k denotes the center vector of the kth hidden neuron and $\|\mathbf{x} - \mu_k\|$ is the Euclidean distance between $\mathbf{x}$ and μ_k; σ_k is the radius or width of the kth hidden neuron.

2.2. Flexible Structure Radial Basis Function Neural Network. The FS-RBFNN is based on the average firing rate of the hidden neurons and the MI intensities between the hidden layer and the output layer. Firstly, the activities of the hidden neuron are evaluated according to the average firing rate. The hidden neurons which have a high firing rate are divided into new neurons. Secondly the MI value is used to adjust the network structure; that is, the value of the MI is used as a measure of the connectivity between the hidden layer and the output layer; connections which have a small MI value will be pruned in order to simplify the structure of the network. Finally the gradient-descent method, which is used to adjust the values of the parameters, ensures the exactitude of the FS-RBFNN.

The main steps of the proposed FS-RBFNN algorithm can be summarized as follows.

Step 1. Create an initial RBFNN consisting of three layers, an input layer, a hidden layer, and an output layer. The number of neurons in the input and output layers is the same as the number of input and output variables in the problem that is being solved. The number of neurons in the hidden layer is randomly generated. Initialize all the parameters: the centers, radii, and connection weights of the RBFNN are all uniformly distributed with a small range.

Step 2. For the input sample $\mathbf{x}(t)$, train the RBFNN using training rule as

$$W(t+1) = W(t) + \dot{W}(t). \tag{3}$$

The centers and radii are adjusted by the gradient method proposed in [13]. The mean squared error (MSE) is defined as

$$E = \frac{1}{2T} \sum_{t=1}^{T} e^2 (t), \tag{4}$$

where T is the number of the training samples.

Step 3. Compute the active firing rate, Af, of the hidden neurons using formula (4). New neurons are inserted according to the activity threshold Af_0. If $\mathrm{Af}_i > \mathrm{Af}_0$, go to Step 4; else go to Step 5. Consider

$$\mathrm{Af}_i = \rho \exp\left(\mathbf{x} - \mu_i\right) \frac{\theta_i(\mathbf{x})}{\sum_{i=1}^{K} \theta_i(\mathbf{x})}, \quad (i = 1, 2, \ldots, K), \tag{5}$$

where Af_i is the active firing of the ith hidden neuron, K is the number of hidden neurons, $\theta_i(\mathbf{x})$ is the output value of the ith hidden neuron, and $\rho \gg 1$ is a positive constant.

Step 4. Split the ith hidden neuron and insert new hidden neurons. The initial parameters of the new inserted neurons are obtained from formulas (5) and (6).

Step 5. If $M(X_i; Y)$, which is calculated by formula (6), is less than the threshold M_0 ($M_0 < 0.05$), go to Step 6. Otherwise, go to Step 7. Consider

$$M(X_i; Y) = \sum_{x,y} p(X_i, Y) \log_2 \frac{p(X_i, Y)}{p(X_i)\, p(Y)}, \tag{6}$$

where $p(X_i, Y)$ is the joint distribution and $p(X_i)$ and $p(Y)$ are the single-variable marginal. In this paper, X_i is the output value of the ith hidden neuron; Y is the network's output.

Step 6. Delete the connection between the hidden neuron X_i and the output neuron Y; update the remaining RBFNN parameters. Find the neuron X' in the hidden layer which has the minimal Euclidean distance between neuron X_i and neuron X'. The parameters of the hidden neuron X' are adjusted as

$$\begin{aligned} \mu'_{X'} &= \mu_{X'} \\ \sigma'_{X'} &= \sigma_{X'} \\ \omega'_{X'} &= \omega_{X'} + \omega_{X_i} \frac{\theta_X(\mathbf{x}(t))}{\theta_{X'}(\mathbf{x}(t))}, \end{aligned} \tag{7}$$

where $\omega_{X'}$ and $\omega'_{X'}$ are the connecting weight of the hidden neurons X' before and after structure adjusting, $\mu_{X'}$ and $\mu'_{X'}$ are the center of the hidden neurons X' before and after deleting neuron X_i, and $\sigma_{X'}$ and $\sigma'_{X'}$ are the radius of the hidden neurons X' before and after deleting neuron X_i.

Step 7. $t = t + 1$; go to Step 2. Stop when $t = T$.

Figure 2 is the flow chart of FS-RBFNN.

3. PCI Failure Probability Prediction

Water cooled reactor fuel is subjected to several operational restrictions in order to secure cladding integrity under various classes of anticipated operational transients. Typically, only a few failures occur during a reactor start-up or Condition 2 transients. They are avoided by controlling the magnitude, and the rate of power increases to maintain the cladding tensile stress below the threshold stress or by design measures that increase the threshold for given ramp conditions. Maximum allowable operating conditions are established on the basis of extensive calculations involving analyses of multiple transients, multiple irradiation histories for every rod in a large portion of a reactor core. Pellet-induced cladding failures occurring during power transients can be classified as follows [5].

SCC is described as follows: Stress corrosion cracking (SCC) is initiated on the inside surface of the cladding due to the sustained strain from pellet-cladding mechanical interaction (PCMI) and the presence of a caustic agents such as iodine and cesium fission products. The tensile stress for this type of defect is below the yield strength of the cladding.

PCMI is described as follows: cladding ductility is exceeded due to strain from pellet thermal expansion and fission gas-induced swelling. The tensile stress required for this type of defect exceeds the yield strength of the cladding. Since PCMI cracks may initiate either on inside or outside cladding surfaces, this failure mechanism also includes outside-in failures, some of which are presently attributed to the local hydriding weakening of the cladding.

Once PCI failures were recognized as a manifestation of PCMI and SCC, it was evident that four factors would be simultaneously necessary for failure to occur: sufficient stress, sufficient time, a susceptible material, and the right chemical environment. However, the four factors are hard to detect during operation or power transients, and the mechanism of the whole PCI-induced clad failure process is so complex, which consists of nuclear dynamics, thermohydraulics, mechanics of materials, and so on. We solve the problem by a "black box method," which only focuses on the inputs and outputs of the system but do not consider its mechanism. The four factors of the PCI failures mentioned before are the results of the power transient and history, not the sources. As for the power transient and history, the power increase (ΔP) and peak power ($P_{\max}$) during power ramp are used to denote the effects of the power transient, and the Burnup of the fuel (BU) is used to denote the effects of the power history. In this way, the model uses ΔP, $P_{\max}$, and BU as inputs to estimate the output PCI by FS-RBFNN.

In this section, the main objective is to develop a PCI failure probability prediction model using the proposed FS-RBFNN. The FS-RBFNN was programmed with Matlab version 8.3 and was run on an Intel(R) Core(TM) i7 with a clock speed of 3.4 GHz and 4 GB of RAM, under a Microsoft Windows 8.1 environment.

The FS-RBFNN can be designed to update its input-output performance, resulting in continuous, online, self-correcting models. In the experiment, the most important parameters affecting PCI are selected: power increase (ΔP) during power ramp, peak power ($P_{\max}$) during power ramp, and Burnup of the fuel (BU) as the input research variables. The network's output vector is the clad condition (defect or nondefect) after power ramp. We use "1" to denote "defect" and "0" to denote "nondefect." The data used in the experiment was collected from Douglas Point Reactor, which is a pressurized heavy water reactor in Canada [14]. 31 defect points and 199 nondefect points are chosen in the $P_{\max}$-BU experimental results, 5 defect points and 15 nondefect points in them are the testing samples named Douglas-1 test,

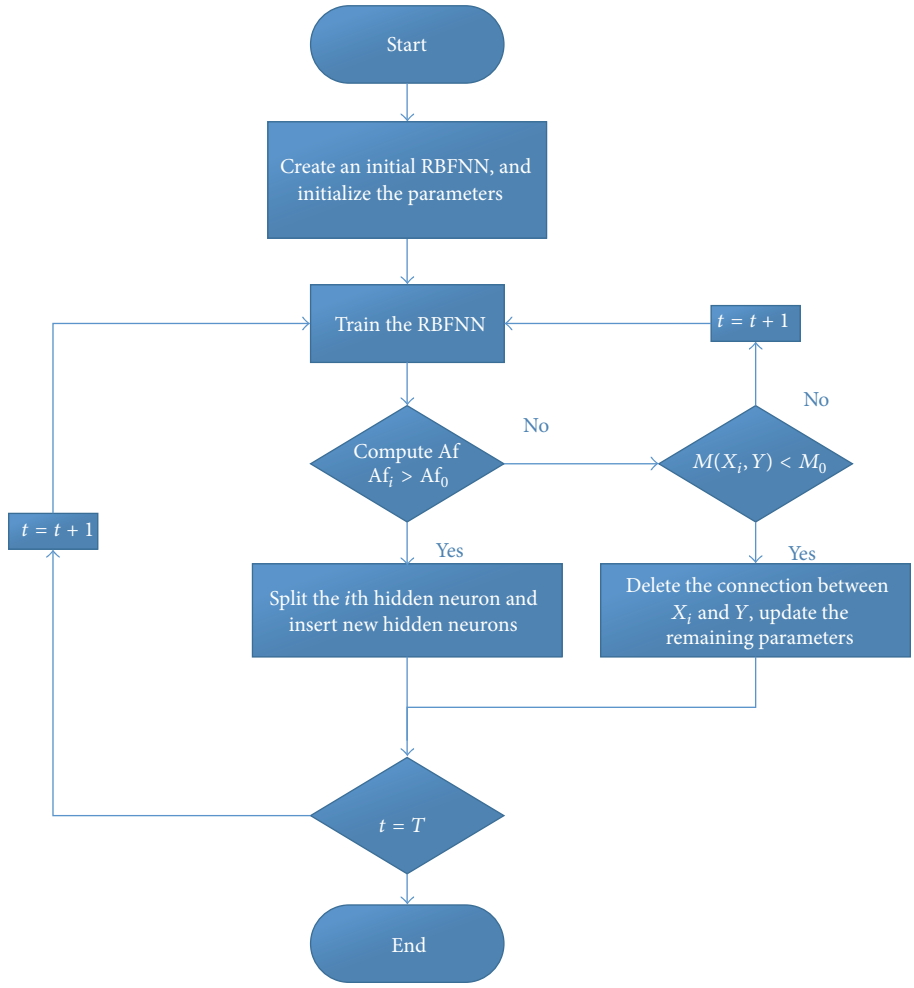

Figure 2: Flow chart of the FS-RBFNN.

and others are training samples named Douglas-1. 29 defect points and 181 nondefect points are chosen in the ΔP-BU experimental results, 5 defect points and 15 nondefect points in them are the testing samples named Douglas-2 test, and others are training samples named Douglas-2.

As the various units of the inputs and output, the samples are normalized as

$$x_{\text{nor}} = \frac{x - x_{\min}}{x_{\max} - x_{\min}}, \tag{8}$$

where x is the actual value, $x_{\min}$ and $x_{\max}$ are the minimum and maximum value, and x_{nor} denotes the normalized value of x.

4. Results and Discussion

4.1. Training and Testing of Douglas-1. First, the data Douglas-1 is trained, the inputs here are $P_{\max}$ and BU, and the output is the clad condition. There are 210 groups of $P_{\max}$-BU-clad condition in Douglas-1. Figure 3 shows the RBFNN training process by Douglas-1.

It can be seen from Figure 3 that the neuron network almost totally converges at the 50th step. The Mean Square Error (MSE) is less than 10^{-28}. The Douglas-1 test is used to test the trained network, and the results are list in Table 1.

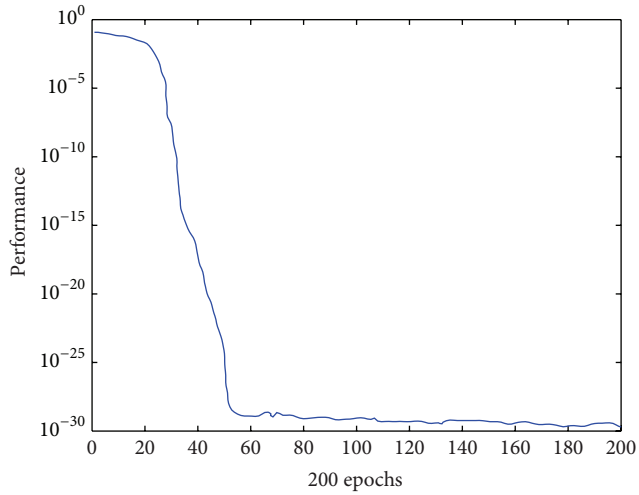

Figure 3: The RBFNN trained by Douglas-1.

Table 1: The Douglas-1 test results of the RBFNN trained by Douglas-1.

Test number	Predicted value	Real value
1	0.6571	1
2	0.3245	1
3	0.2431	1
4	0.8250	1
5	0.3045	1
6	$2.1451e-19$	0
7	$1.5672e-20$	0
8	$6.2145e-19$	0
9	$4.1994e-21$	0
10	$6.0145e-20$	0
11	$4.1789e-19$	0
12	$5.0212e-19$	0
13	$8.2351e-19$	0
14	$3.5612e-20$	0
15	$2.4791e-20$	0
16	$1.0367e-21$	0
17	$6.3299e-19$	0
18	$3.1274e-19$	0
19	$8.4413e-19$	0
20	$7.5123e-19$	0

Table 2: The Douglas-2 test results of the RBFNN trained by Douglas-2.

Test number	Predicted value	Real value
1	0.1345	1
2	0.9745	1
3	0.0156	1
4	0.6825	1
5	0.4245	1
6	$2.4461e-18$	0
7	$8.4612e-20$	0
8	$5.2130e-19$	0
9	$4.3214e-20$	0
10	$6.6415e-19$	0
11	$8.1609e-19$	0
12	$4.3482e-19$	0
13	$7.1971e-21$	0
14	$3.5642e-19$	0
15	$1.7993e-20$	0
16	$1.0497e-21$	0
17	$8.3319e-18$	0
18	$7.1644e-19$	0
19	$8.2013e-20$	0
20	$6.6643e-20$	0

Tests numbers 1–5 are the defect points, and tests numbers 6–20 are the nondefect points in the literature. The real value in Table 1 is the real output of clad condition, while the predicted value is the output from the RBFNN. It can be seen that the predicted values are not equal to the real value. But they vary in the order of magnitude, the predicted values of numbers 1–5 are in the range of 10^{-1}–10^{0} (real value = 1), and those of numbers 6–20 are in the range of 10^{-21}–10^{-19} (real value = 0). That means the RBFNN can classify the defect and nondefect points effectively.

4.2. Training and Testing of Douglas-2. As to the training of the data Douglas-2, the inputs are ΔP and BU and the output is the clad condition. There are 190 groups of ΔP-BU-clad condition in Douglas-2. Figure 4 shows the RBFNN training process by Douglas-2.

It can be seen from Figure 4 that the neuron network converges at the about 100th step, which is slower than that in Figure 3. The MSE is approximately 10^{-28}. The Douglas-2 test is used to test the trained network, and the results are listed in Table 2.

The results in Table 2 are similar to Table 1, while the test number 3's prediction value is 0.0156 very small than other defect points. When it comes to the nondefect points (test numbers 6–20), the prediction results are in the range of 10^{-21}–10^{-18} (real value = 0), which are similar to their real value. Therefore, the method also does well on Douglas-2.

Tables 1 and 2 show that the prediction results correspond to the experimental data. That means the PCI failure prediction by using FS-RBFNN model is feasible and that the results calculated by this model are accurate. The average training time is less than 4 seconds, which is rapid enough and more accurate for our problem. The experiment data contain two groups; one is the relationship between $P_{\max}$ and BU, and the other is the relationship between ΔP and BU. As the two relationships were listed separately in the literature, the RBFNN models are trained separately, too.

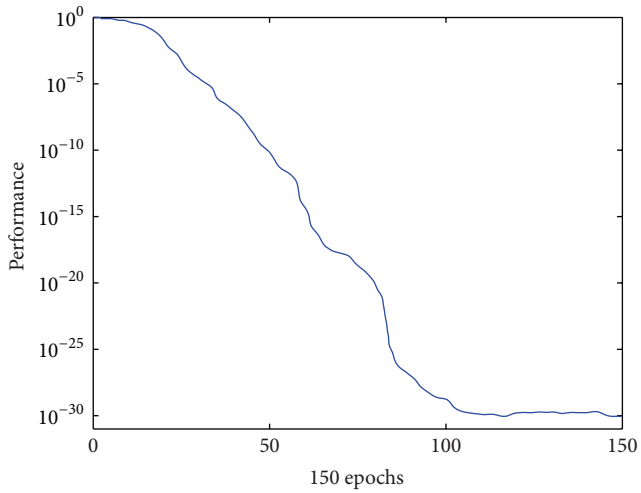

Figure 4: The RBFNN trained by Douglas-2.

5. Conclusions

In this paper, a self-organizing neural network named FS-RBFNN is used to predict the PCI failure probability. Based on its advantages of varying its hidden layer dynamically and

reducing the calculation time, this neural network model can maintain its prediction accuracy and efficiency, which are suitable features for online calculation when a reactor is operating. Although other mechanistic models are probably more accurate than the present neural network model, the benefit of the latter is the faster calculation with moderate accuracy. Comparing to a simple criterion, the FS-RBFNN method can be used by the input data processing instead of the PCI mechanism analysis. The calculation results based on the data from existing literature demonstrate the effectiveness of the present method. According to the rapid and accurate prediction results, the PCI failure condition after a power ramp can be obtained. Therefore, it is beneficial for early warning and dealing with the possible accident of clad failure. Finally, it should be stressed that the applicability of FS-RBFNN relies on the availability of large number of experimental data.

Competing Interests

The authors declare that there is no conflict of interests regarding the publication of this paper.

Acknowledgments

This work was supported by the National Science Foundation of China under Grant 11405125, China Postdoctoral Science Foundation Funded Project under Grant 2014M562420, and the Fundamental Research Funds for the Central Universities.

References

[1] B. Cox, "Pellet clad interaction (PCI) failures of zirconium alloy fuel cladding—a review," *Journal of Nuclear Materials*, vol. 172, pp. 249–292, 1990.

[2] T. Alam, M. K. Khan, M. Pathak, K. Ravi, R. Singh, and S. K. Gupta, "A review on the clad failure studies," *Nuclear Engineering and Design*, vol. 241, no. 9, pp. 3658–3677, 2011.

[3] S. A. Nikulin and A. B. Rozhnov, "Corrosion cracking of zirconium cladding tubes (a review). I. Methods of study and mechanisms of fracture," *Metal Science and Heat Treatment*, vol. 47, no. 1-2, pp. 71–79, 2005.

[4] EPRI, "PCI analyses and startup ramp rate recommendations for westinghouse fuel in exelon PWRs," EPRI Report-Product 1012915, 2006.

[5] D. V. Paramonov, "Pellet-cladding interaction probability assessment model," *Journal of Pressure Vessel Technology*, vol. 134, no. 1, Article ID 011401, 2012.

[6] B. Michel, J. Sercombe, and G. Thouvenin, "A new phenomenological criterion for pellet-cladding interaction rupture," *Nuclear Engineering and Design*, vol. 238, no. 7, pp. 1612–1628, 2008.

[7] B. Michel, J. Sercombe, G. Thouvenin, and R. Chatelet, "3D fuel cracking modelling in pellet cladding mechanical interaction," *Engineering Fracture Mechanics*, vol. 75, no. 11, pp. 3581–3598, 2008.

[8] J. Sercombe, I. Aubrun, and C. Nonon, "Power ramped cladding stresses and strains in 3D simulations with burnup-dependent pellet-clad friction," *Nuclear Engineering and Design*, vol. 242, pp. 164–181, 2012.

[9] H.-G. Han, Q.-L. Chen, and J.-F. Qiao, "An efficient self-organizing RBF neural network for water quality prediction," *Neural Networks*, vol. 24, no. 7, pp. 717–725, 2011.

[10] G. Neves, S. F. Cooke, and T. V. P. Bliss, "Synaptic plasticity, memory and the hippocampus: a neural network approach to causality," *Nature Reviews Neuroscience*, vol. 9, no. 1, pp. 65–75, 2008.

[11] S. Krivov, R. E. Ulanowicz, and A. Dahiya, "Quantitative measures of organization for multiagent systems," *BioSystems*, vol. 69, no. 1, pp. 39–54, 2003.

[12] N. Mai-Duy and T. Tran-Cong, "Approximation of function and its derivatives using radial basis function networks," *Applied Mathematical Modelling*, vol. 27, no. 3, pp. 197–220, 2003.

[13] J.-F. Qiao and H.-G. Han, "A repair algorithm for radial basis function neural network and its application to chemical oxygen demand modeling," *International Journal of Neural Systems*, vol. 20, no. 1, pp. 63–74, 2010.

[14] V. Pasupathi, J. S. Perrin, E. Roberts et al., "Determination and microscopic study of incipient defects in irradiated power reactor fuel rods," Tech. Rep. NP-812, Electric Power Research Institute, 1978.